UC Irvine
UC Irvine Previously Published Works

Title

Dynamic Simulation of a Stationary Proton Exchange Membrane Fuel Cell System

Permalink

https://escholarship.org/uc/item/2c8580x8

Journal

Journal of Electrochemical Energy Conversion and Storage, 6(4)

ISSN

1550-624X

Authors

Min, Kyoungdoug
Kang, Sanggyu
Mueller, Fabian
et al.

Publication Date

2009-11-01

DOI

10.1115/1.3008029

Copyright Information

Peer reviewed

Dynamic Simulation of a Stationary Proton Exchange Membrane Fuel Cell System

Kyoungdoug Min[1]
e-mail: kdmin@snu.ac.kr

Sanggyu Kang

School of Mechanical and Aerospace
Engineering,
Seoul National University,
Gwanakgu, Seoul 151-742, Republic of Korea

Fabian Mueller

John Auckland

Jacob Brouwer

Mechanical and Aerospace Engineering,
Department National Fuel Cell Research Center,
University of California,
Irvine, CA

A dynamic model of a stationary proton exchange membrane (PEM) fuel cell system has been developed in MATLAB-SIMULINK®. The system model accounts for the fuel processing system, PEM stack with coolant, humidifier with anode tail-gas oxidizer, and an enthalpy wheel for cathode air. Four reactors are modeled for the fuel processing system: (1) an autothermal reformation (ATR) reactor, (2) a high temperature shift (HTS) reactor, (3) a low temperature shift (LTS) reactor, and (4) a preferential oxidation reactor. Chemical kinetics for ATR that describe steam reformation of methane and partial oxidation of methane were simultaneously solved to accurately predict the reaction dynamics. The chemical equilibrium of CO with H_2O was assumed at HTS and LTS reactor exits to calculate CO conversion corresponding to the temperature of each reactor. A quasi-one-dimensional PEM unit cell was modeled with five control volumes for solving the dynamic species and mass conservation equations and seven control volumes to solve the dynamic energy balance. The quasi-one-dimensional cell model is able to capture the details of membrane electrode assembly behavior, such as water transport, which is critical to accurately determine polarization losses. The dynamic conservation equations, primary heat transfer equations and equations of state are solved in each bulk component, and each component is linked together to represent the complete system. The model predictions well matched the observed experimental dynamic voltage, stack coolant outlet temperature, and catalytic partial oxidation (CPO) temperature responses to perturbations. The dynamic response characteristics of the current system are representative of a typical stationary PEM fuel cell system. The dynamic model is used to develop and test a proportional-integral (PI) fuel flow controller that determines the fuel flow rate to maintain the uniform system efficiency. The dynamic model is shown to be a useful tool for investigating the effects of inlet conditions, load, and fuel flow perturbations and for the development of control strategies for enhancing system performance.
[DOI: 10.1115/1.3008029]

Keywords: dynamic modeling, stationary PEM fuel cell system, reformer, PI controller

Introduction

PEM fuel cell (PEMFC) technology has received attention as a promising future stationary power source because of its high power density, low temperature operation, quick start-up, system robustness, the ability to respond to rapid changes in power demand, and low emissions [1–4]. Several stationary PEMFC system products have been introduced into the market recently [5,6], most using pure hydrogen fuel. But since hydrogen is not readily available at reasonable prices today, much research has been carried out to develop small-scale fuel processing systems to locally generate hydrogen [7–11].

System level dynamic modeling is useful for improving system integration, system efficiency, and developing and optimizing control strategies for transient operating conditions. Only a few researchers have reported on system level dynamic modeling of the stationary PEM fuel cell system. On the other hand, component level dynamic models are more abundant, with a few addressing reformer reactors [12,13] and many others simulating the fuel cell component. Fuel cell and stack level transient modeling include the bulk dynamic model of a PEM fuel cell developed by Shan and Choe, and Yuyao and Choe investigated the mechanisms

of PEMFC dehydration [14,15]. Another bulk dynamic model used for developing a control system was presented by Yerramalla et al. using MATLAB-SIMULINK® [16]. The dynamic characteristics of water transport in a PEMFC was elucidated by Pukrushpan et al. [17]. Xue et al. developed a dynamic PEMFC model that could predict the effects of temperature, gas flow, and capacitance on system transient behavior [18]. A simplified dynamic model of a PEM fuel cell considering the effect of cathode kinetics was recently developed by Ceraolo et al. using MATLAB/SIMULINK® [19]. While a one-dimensional dynamic model is useful for investigating the dynamic response of PEMFC, it cannot capture the distribution of current, species, temperature, and membrane water content in the cell. More recently, a 3D dynamic model of a PEM fuel cell has been developed by Wang and Wang to study important transient phenomena of the electrochemical double layer discharging, gas transport through gas diffusion layer (GDL) and membrane hydration [20]. The transient multidimensional model of Um and Wang elucidated the electrochemical kinetics, current distribution, hydrodynamics, and multicomponent transport [21]. Guilin et al. represented a three-dimensional computational PEM fuel cell model with conventional and interdigitated flow fields [22]. The three-dimensional mixed-domain PEM fuel cell model of Meng, which integrates the various transport phenomena, has been applied to investigate the effects of the fully coupled transport phenomena on the cell performance, current distribution, and net water transfer across the membrane [23]. The three-dimensional computational fluid dynamics (CFD) model of Maher et al. accounts for detailed species mass transport, heat transfer in
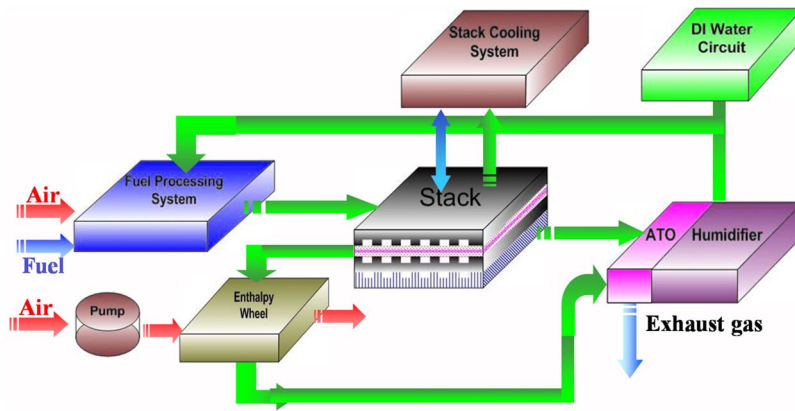
Fig. 1 Schematic of the stationary fuel cell system model

the solids as well as in the gases, potential losses in the gas diffusion layers and membrane, electrochemical kinetics, and the transport of water through the membrane [24]. Wang and Wang presented the numerical simulations of a single-channel PEFC with Gore® 18 μm and Nafion® 112 membranes for investigating the dynamic response under current density step changes with focus primarily on dry cell operation [25]. Mueller et al. presented a quasi-three-dimensional dynamic model that can capture both the dynamic response characteristics and some effects of cell geometry in a PEMFC model that is simplified enough to be useful in system level simulation and control system development [26]. A three-dimensional transient model including the two phase flow, species transport, heat transfer, and electrochemical processes was developed by Wang and Wang to study the dynamics of gas diffusion layer dewetting and its polymer electrolyte fuel cell performance [27]. Few of these dynamic PEMFC models are used to study fully integrated PEMFC systems.

In the modeling of a fuel processing system, few studies have been reported in the field of reactor design and simulation. Barrio et al. developed a one-dimensional quasihomogeneous reactor model that can be used to investigate the significant effects of gas feeding on reactor performance [8]. Pukrushpan recently published a system level model of a natural gas fuel processor system and PEM stack for automotive application [28]. However the chemical reaction of methane was simplified by using curve fitting of a steady-state simulation result, and the membrane electrode assembly (MEA) water content was simply estimated as the average of the anode and cathode humidity.

The objectives of this paper are to present the development of a system level dynamic model of a stationary PEM fuel cell system in MATLAB-SIMULINK®, to evaluate the model by comparison to experimental data from a Plug Power (Latham, New York) system, and to demonstrate the model by exploring some control strategies. The model simulates the chemical kinetics in the CPO and the detailed electrochemical performance of the PEMFC stack. The system level model is useful for investigating physical system level transient response characteristics and for developing and optimizing control strategies. The primary components of the physical system are: fuel processing system, PEMFC stack, humidifier with anode tail-gas oxidizer (ATO), de-ionized water circuit, power electronics and conditioning system, and balance of plant (BOP). The dynamic simulation was compared with the experimental data performed during two different load change perturbations. Finally, a controller was implemented in the model to manipulate the fuel flow rate to improve system efficiency.

System Model

A dynamic system model was developed based on the Plug Power GenSys™ stationary fuel cell system. The GenSys™ is a 5 kV A system that operates on natural gas that is processed to produce pure hydrogen before being sent to an 88 cell PEM fuel cell stack [29]. The system schematic is shown in Fig. 1. The system model accounts for the major components of the system including the fuel processing system with humidification, the enthalpy wheel, the PEM stack with coolant, and ATO. System components are modeled individually and integrated to form a system. Individual components are discretized into control volumes, in which dynamic conservation equations are applied and mass and heat transfer amongst control volumes are captured.

Major Assumptions. The major modeling assumptions are as follows:

1. Only the following major species are considered in the model: CH_4, CO, CO_2, H_2, H_2O, N_2, and O_2.
2. All gases are ideal gases [30].
3. Control volumes are characterized by a single lumped temperature, pressure, and set of species mole fractions.
4. A uniform gas pressure is assumed. The pressure drop along the gas flow channels and GDL are assumed to be negligible [30].
5. The solid GDL and MEA have a lumped temperature.
6. Each cell in the stack is assumed to operate identically, so that a single unit cell simulation is taken as representative and used to calculate full stack performance [30,31].
7. The fuel cell electrodes are assumed to be perfect conductors from which an equipotential electrode surface can be assumed [32].
8. Quasisteady electrochemistry is assumed since the electrochemistry is rapidly occurring at time scales on the order of 10^{-3} s [20,33].
9. A single activation polarization equation is used to capture the effects of all physical and chemical processes that polarize the charge transfer process.
10. All reactants generate their ideal number of electrons, and no fuel or oxidant crosses the electrolyte [28].

Conservation Equations. The temperature, species mole fractions, and water content of control volumes throughout the system model are determined from first principles conservation equations. The form of the conservation equations utilized in control volumes throughout the model are of similar form. The general conservation equations utilized are described here. Details regarding each of the component models are provided thereafter.

Energy Conservation. Dynamic energy conservation equations are used to solve for the temperature in each control volume. Temperatures of solid control volumes are determined by solving the following ordinary differential equation (ODE):
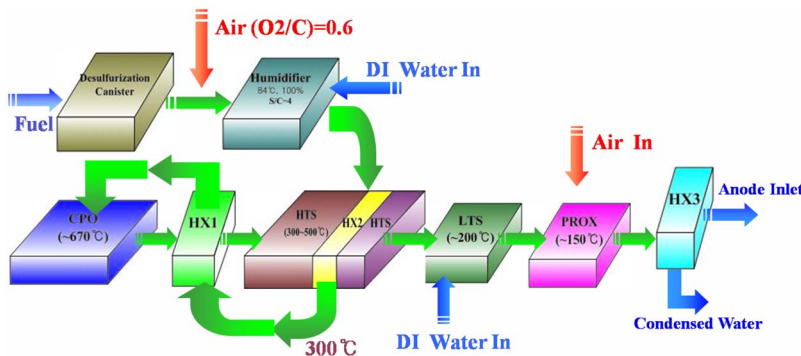
Fig. 2 Schematic of the fuel processing system

$$\rho V C \frac{dT}{dt} = \sum \dot{Q}_{in}$$

The temperatures of gas channel and coolant control volumes are determined by solving the dynamic energy conservation equation in the form

$$N C_V \frac{dT}{dt} = \sum \dot{N}_{in} h_{in} - \sum \dot{N}_{out} h_{out} + \sum \dot{Q}_{in}$$

where h is the enthalpy of fluid or gas and N is the number of moles in the control volume.

Species Conservation. Species mole fractions at the exit of each bulk fluid control volume are determined from the dynamic species conservation equation

$$\frac{d(N\vec{X})}{dt} = \dot{N}_{in}\vec{X}_{in} - \dot{N}_{out}\dot{X}_{out} + \sum \vec{\Phi}$$

where $\vec{X}$ is the species mole fraction vector and $\vec{\Phi}$ is the species diffusion flux from adjacent control volumes, where applicable.

Fuel Processing System. The primary purpose of the fuel processing system is to chemically convert hydrocarbon fuel (such as CH_4) into a fully humidified and sufficiently purified reformate for electrochemical conversion in the PEMFC stack. The schematic of the fuel processing system and the general operating conditions used in the current work are shown in Fig. 2. The fuel processing system of the Plug Power stationary fuel cell system is comprised of a desulfurization bed, the main reactor that contains the ATR and HTS reactors, and separate LTS and preferential oxidation (PROX) reactors.

In the system model four reactors are simulated: (1) ATR, (2) high temperature shift reactor (HTS), (3) low temperature shift reactor (LTS), and (4) PROX reactor. The ATR operates autothermally by catalytic promotion of both steam reforming (SR) and partial oxidation (POX) reactions with the feed of fuel, water and air. The ATR produces a reformate containing H_2, CO, H_2O, and CO_2. The shift and PROX reactors are required to promote the complete reaction of CO with H_2O over a catalyst to produce CO_2 and additional hydrogen.

Each of the reactors is discretized into gas and solid catalyst control volumes. Heat transfer between the gas and catalyst control volumes is resolved as convective heat transfer,

$$Q_g = h_c \cdot A_c \cdot V_c \cdot (T_g - T_c)$$

Along with the energy conservation of the gas and solid, this makes it possible to capture thermal transients in each of the reactors. Chemical kinetics or equilibrium calculations, as noted for each reactor below, are then used to determine the reactor species mole fractions.

The chemical kinetics of ATR consist of reactions that take place in steam reforming and partial oxidation of methane. A

widely used three-step SR mechanism for reaction of methane over a nickel supported catalyst ($Ni/MgAl_2O_4$) is used [34]. These chemical kinetics are combined with a three-step POX mechanism for the reaction of methane and air over a nickel supported catalyst (Ni/Al_2O_3) to simulate the complete ATR chemistry [35].

In the high temperature and low temperature shift reactors, the chemical equilibrium of CO with H_2O is assumed at the reactor exit temperature and pressure conditions. This makes it possible to calculate CO conversion corresponding to the temperature of each reactor. To lower the temperature of the HTS reactor products before entering the LTS reactor, the HTS effluent is cooled and rehumidified by introducing de-ionized water prior to entering the LTS. It is assumed that the energy to cool the HTS exhaust gas temperature is completely supplied by the latent heat of the de-ionized water. In the PROX reactor it is assumed that additional air is supplied in the proper amount to completely oxidize the remaining CO at a selectivity of 0.5 over the PROX catalyst.

ATO With Humidifier. The ATO and humidifier exist as one assembly and work together to produce a 100% humidified fuel and air mixture for use in the fuel processing system. The ATO with humidifier is modeled as two separated gas control volumes with ideal heat transfer between the two volumes. In the ATO the excess hydrogen from the PEM fuel cell stack is oxidized in a catalytic reaction to provide heat for the humidifier. 100% oxidation of hydrogen is assumed in the model. De-ionized water is sent to the humidifier to control the wet-bulb temperature of the fuel/air mixture to a specific set point, which controls the steam-to-carbon ratio (SCR) as a constant. All the heat required to vaporize and preheat the water in the humidifier is extracted from the ATO product stream.

Enthalpy Wheel. The enthalpy wheel is used to supply sensible energy and moisture to incoming air from the exhausted cathode air. The sensible energy transfer occurs simply because the wheel heats up in the exhausted cathode air and then transfers the heat to the incoming air stream. Moisture is transferred in a similar manner. It is assumed that the enthalpy wheel is quasi-steady. The continuity and energy equations for both incoming air and the exhausted cathode air were applied.

The dynamic conservation equations, primary heat transfer equations, and equations of state are solved in each bulk component, and each component is linked together to represent the complete system. Measurements of complete system physical characteristics, such as weight, volume, and material properties, were used to relate the model directly to a fully functional system, and performance data were acquired for model evaluation.

PEM Fuel Cell Stack. The fuel cell was modeled as in Mueller et al. [26] without the flow direction discretization. That is, the fuel cell stack was only discretized in the flow perpendicular direction, which is shown in Figs. 3 and 4. The same electrochemi-
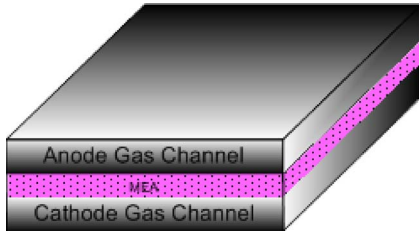
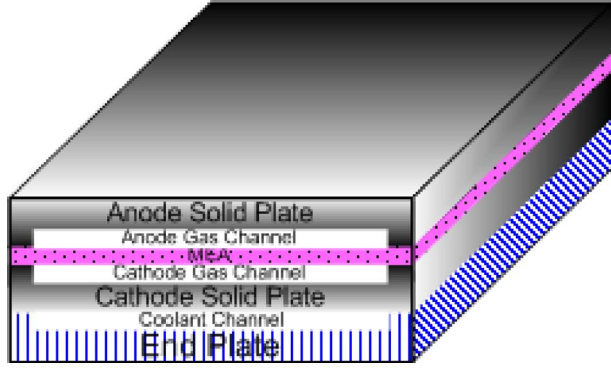**Fig. 3 Control volumes for species conservation of PEM unit cell (not drawn to scale)**

Fig. 4 Control volumes for energy conservation in the PEM unit cell (not drawn to scale)

cal, water transport, and heat transfer equations were used in the fuel cell control volumes as in Mueller et al. [26]. Consequently the fuel cell model is not described in detail herein.

The fuel cell is discretized perpendicular to the flow through a unit cell of the fuel cell stack, which is an approach similar to that used by Yuyao and Choe [15] and Freunberger et al. [30]. The primary components of the fuel cell are discretized perpendicularly into seven control volumes, using five types of control volumes: (1) solid plate, (2) bulk gas, (3) GDL, (4) MEA, and (5) coolant.

It was found most important to resolve the fuel cell in the flow perpendicular direction to accurately model local species at the triple phase boundary and to capture membrane hydration dynamics, which largely affect the electrochemical performance of the fuel cell. It is important to resolve the flow perpendicular direction because the gas from the gas channel diffuses through the GDL to the triple phase boundary, between the GDL and the MEA. Significant species gradients can exist between the bulk gas and triple phase boundary. Diffusion fluxes and osmotic water transport to the GDL control volume are determined for the boundary between the electrolyte and GDL control volume. Without a flow perpendicular discretization, water transport cannot be accurately resolved. A flow perpendicular discretization makes it possible to more accurately model the membrane hydration, which is critical to accurately determine overall performance and polarization losses.

While separate GDL and MEA control volumes are essential to resolve the water transport and concentration gradients within the fuel cell, the GDL and MEA can be lumped together into one perpendicular control volume to resolve the perpendicular temperature profile.

The species transport from gas channel to GDL accounts for the convection driven and diffusion in the GDL. The mass transport coefficient at the gas channel and GDL interface is obtained based on the Reynolds analogy between heat and mass transfer,

$$g_m = \frac{Sh \cdot D_m}{L}$$

The diffusion coefficients for species are a function of temperature and pressure and are modified via the Bruggeman correlation to account for the effects of porosity and tortuosity in the GDL [36].

Water Transport

As the water content in the membrane strongly affects the ionic conductivity, dynamic model should capture the details of water behavior in the MEA. Two types of water molecule transport from anode or cathode GDL to electrolyte are considered: (1) the electro-osmotic drag and (2) backdiffusion due to concentration gradient between two control volumes. The amount of water molecules dragged from the anode-electrolyte interface to the cathode-electrolyte interface is proportional to the current density and the electro-osmotic drag coefficient.

$$\dot{n}_{osmotic} = n_d \cdot \frac{i}{F}$$

The osmotic drag coefficient, n_d, is calculated from the membrane water content, λ, which depends on the water activity, a [37]

$$n_d = 0.0029\lambda^2 + 0.05\lambda - 3.4 \times 10^{-19}$$

$$\lambda = \begin{cases} 0.043 + 17.81a - 39.85a^2 + 36a^3 & \text{for } 0 < a \leq 1 \\ 14 + 1.4(a-1) & \text{for } 1 \leq a \leq 3 \end{cases}$$

The water activity is calculated by

$$a = \frac{X_{H_2O}P}{P_{sat}}$$

The water diffusion due to the concentration gradient between GDLs and electrolyte control volume is calculated by

$$\dot{n}_{diff} = D_w \frac{dc}{dx}$$

The diffusion coefficient of water in the electrolyte, D_w, is calculated from the empirical equation [37]

$$D_w = D_\lambda \cdot \exp\left[2416 \left(\frac{1}{303} - \frac{1}{T} \right) \right]$$

$$D_\lambda = \begin{cases} 10^{-6} & \text{for } \lambda < 2 \\ [1 + 2 \cdot (\lambda - 2)] \times 10^{-6} & \text{for } 2 \leq \lambda \leq 3 \\ [3 - 1.67 \cdot (\lambda - 3)] \times 10^{-6} & \text{for } 3 < \lambda < 4.5 \\ 1.25 \times 10^{-6} & \text{for } 4.5 \leq \lambda \end{cases}$$

It is assumed that the water is produced in the cathode GDL, which is calculated by

$$\dot{n}_{water} = M_{H_2O} \cdot \frac{I}{2nF}$$

Electrochemical Model

The fuel cell voltage in the model is calculated by subtracting activation polarization and Ohmic polarization from the Nernst potential. The Nernst equation is solved for the anode and cathode GDL partial pressures, and the reversible potential dependence was accounted for by solving the dependence of the Gibbs free energy on temperature. As the partial pressure of H_2, O_2, and H_2O at the GDL were used, the concentration polarization was excluded

$$V_{cell} = V_{Nernst} - \eta_{act} - \eta_{Ohm}$$

$$V_{Nernst} = -\frac{\Delta G(T)}{nF} + \frac{R_u T}{nF} \ln \left(\frac{P_{H_2} \cdot P_{O_2}^{1/2}}{P_{H_2O}} \right)$$

Fuel flow	25 SLPM	S/C ratio	4
Air/C ratio	0.6	O_2 utilization	0.5
Current	50.5 A	dc voltage	64.25 V
Inlet air temperature	26°C	Inlet CPO temp.	450°C

Activation Polarization

Due to the slowness of the reactions taking place on the anode and cathode surfaces, a proportion of voltage generated is lost during the electrochemical reaction. However the reaction of hydrogen oxidation at the anode is much faster than that of oxygen reduction at the cathode, it is assumed that the activation loss is only considered at the cathode and is described by the Tafel equation [38],

$$\eta_{act} = a \ln \frac{i}{i_o}, \quad a = \frac{R_u T}{2\alpha F}$$

Ohmic Polarization

The Ohmic polarization is due to the electrical resistance of the electrodes and polymer membrane. The voltage drop is simply proportional to current density

$$\eta_{Ohm} = i \cdot \frac{t}{\kappa}$$

The proton conductivity in the membrane has been correlated by Springer et al. [37]

$$\kappa = (c_1 \lambda - c_o) \cdot \exp\left[1268 \left(\frac{1}{303} - \frac{1}{T} \right) \right]$$

Results and Discussion

Steady State. The integrated system model developed in this work simulates a GenSys™ Fuel Cell system of Plug Power. Constants for the fuel cell polarization were tuned to a single point (labeled "reference point") which operating conditions are shown in Table 1. Polarization constants are then held constant for all other conditions simulated. To make the comparison, the inlet fuel flow rate is set to 25 SLPM. The steam-to-carbon ratio and air-to-carbon ratio are each set at 4. The inlet air temperature and inlet CPO temperature are 26°C and 450°C, respectively. Simulation results of polarization curve are compared with the experimental data shown in Fig. 5. Simulation results well predict the experimental data.

Table 2 shows temperatures of reactors and species mole fractions in the fuel processing system. Hydrogen mole fraction in the CPO is about 0.266, and all fuel was almost converted to CO, H_2, and CO_2. Due to the high S/C ratio, the water mole fraction is relatively high in the CPO. As the reformate flows through HTS and LTS, 99% of CO is removed. The remaining CO is fully converted in the PROX, with hydrogen and water mole fractions being 0.25 and 0.48, respectively, due to the addition of water to cool down the reformate before the LTS.

As the reformate is cooled down to 68°C in a heat exchanger before entering into the anode, 54% of the water vapor is condensed out and the hydrogen mole fraction is increased to 0.33. As the water vapor in the exhaust cathode air is predicted as fully humidified, the relative humidity of the inlet air after passing the enthalpy wheel is also predicted to be 100%. Thus, both anode and cathode inlets are fully humidified. Hydrogen utilization is estimated at about 0.74, and the exhaust hydrogen is completely burned in the ATO to provide heat for the humidifier. Note that measured stack coolant flow rate and temperature of stack coolant inlet were fixed for all computations.
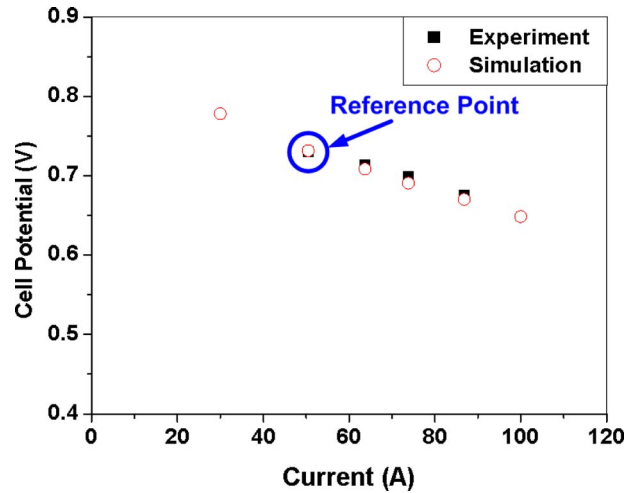

Fig. 5 Comparison between experimental and simulated polarization curves

Transient

Case 1. The first set of dynamic simulation results (Case 1) are presented for a perturbation that lowers the system current from 86.5 A to 50.6 A. Measured system current and fuel flow rate from the Plug Power stationary fuel cell system for the Case 1 perturbation are shown in Fig. 6. Until 14,000 s, the system was operated at a steady-state current demand of 86.5 A and then the current was reduced to 50.6 A over a period of 640 s. These values were used in the model as the dynamic perturbation of the system. The dynamic model was first allowed to reach steady state at a dc current of 86.5 A before the perturbation of system current was applied.

A comparison of system dc voltage and dc power is shown Fig. 7. During the transient state, the simulated dc voltage and power are well matched with the experimental results. As the system current is decreased, the system voltage is increased from 59.6 V to 65.4 V due to decrease in ohmic and polarization losses. System efficiency based on the dc power is shown in Fig. 8. The system efficiency is slightly decreased about 1–2% during the transient state, which can also be found in the simulation result of hydrogen. The hydrogen utilization is decreased from 0.74 to 0.68 during the transient. Even though the hydrogen utilization is decreased a little after the transient, the system efficiency based on stack dc power is not much affected due to increase in the PEM stack efficiency. Thus the system efficiency could be improved by slightly reducing the fuel flow rate to improve the hydrogen utilization.

Temperatures of stack coolant outlet and CPO in the fuel processing system reactors are shown in Figs. 9 and 10, respectively. The temperature of the stack coolant outlet is very important to affect the stack efficiency. During the transient the temperature of the stack coolant outlet is decreased from 70°C to 66°C and then reaches 68°C. Simulation results of the dynamic behavior of the CPO temperature quite well predict the experimental results, and the CPO temperature is increased to about 20°C due to the decrease in fuel flow rate. The hydrogen mole fraction in the fuel processing system during the transient was not much affected because the steam-to-carbon ratio was maintained at around 4. The model predictions well characterize the observed dynamic CPO temperature and stack coolant outlet temperature observations of the experiment.

Case 2. Figure 11 shows a second system perturbation in dynamic current demand, which changes over a period of 1200 s with a 50% decrease in 100 s followed by a 175% increase and a decrease back to the original steady state. The predicted dc power,

Table 2 Simulation results for species mole fractions and reactor temperatures in the fuel processing system

	Inlet condition	CPO	HTS	LTS	PROX	Anode inlet
Flow (kmol/s)	8.83×10^{-5}	1.04×10^{-4}	1.04×10^{-4}	1.25×10^{-4}	1.25×10^{-4}	9.44×10^{-5}
CH_4	0.1355	4.5×10^{-5}	4.5×10^{-5}	4.5×10^{-5}	0	0
CO	0	0.03776	0.0109	0.00039	0	0
CO_2	0	0.0702	0.09702	0.0896	0.0902	0.119
H_2	0	0.2659	0.2921	0.2523	0.2516	0.3335
H_2O	0.542	0.3827	0.356	0.454	0.4544	0.2768
N_2	0.2547	0.2437	0.2437	0.203	0.204	0.2704
O_2	0.06775	3.4×10^{-4}	3.4×10^{-4}	3.3×10^{-4}	0	0
Temperature	84°C	744°C	456°C	202.3°C	168°C	68°C
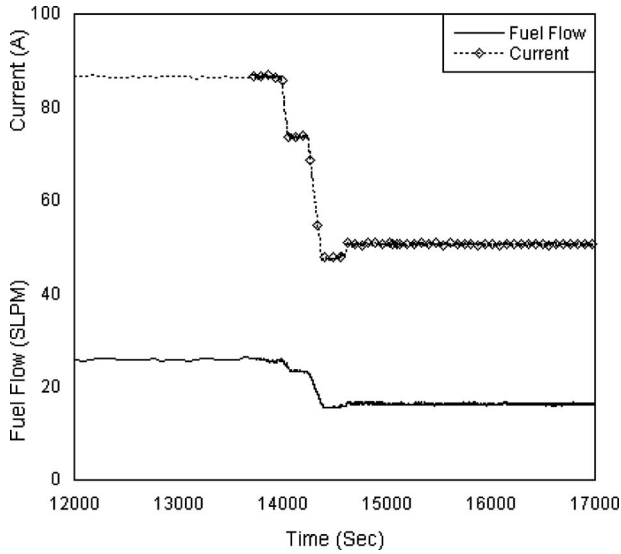
Fig. 6 dc current and fuel flow rate perturbations of Case 1
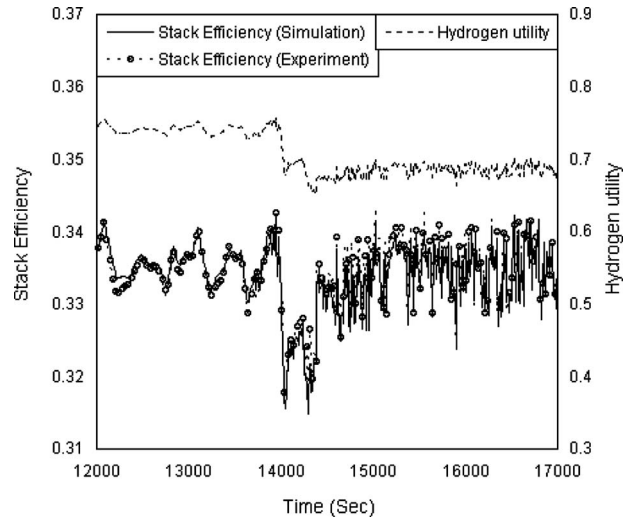

Fig. 8 Comparison of the experimental and simulated stack efficiency and hydrogen utilization during the transient of Case 1
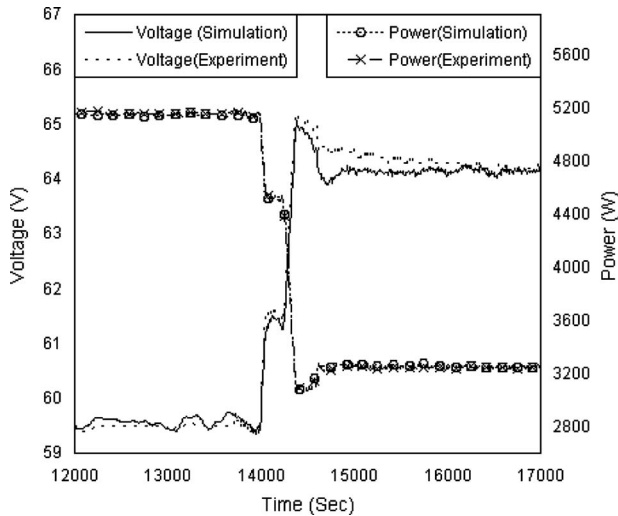

Fig. 7 Comparison of the experimental and simulated transient response of stack voltage and dc power to the Case 1 perturbation
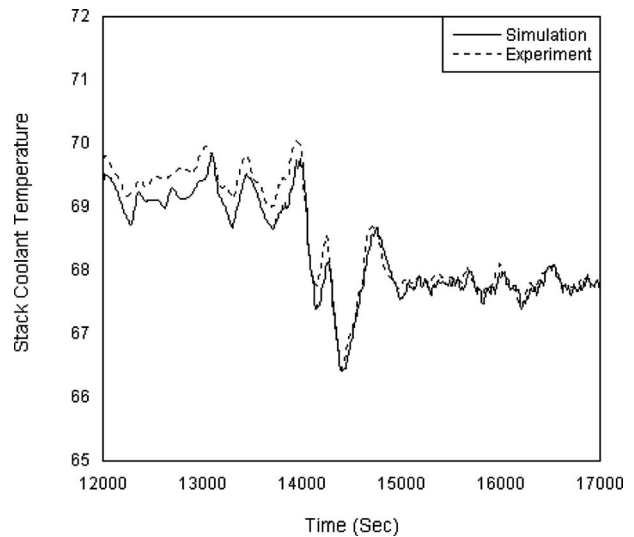

Fig. 9 Comparison between the experimental and simulated stack coolant outlet temperatures during the transient of Case 1
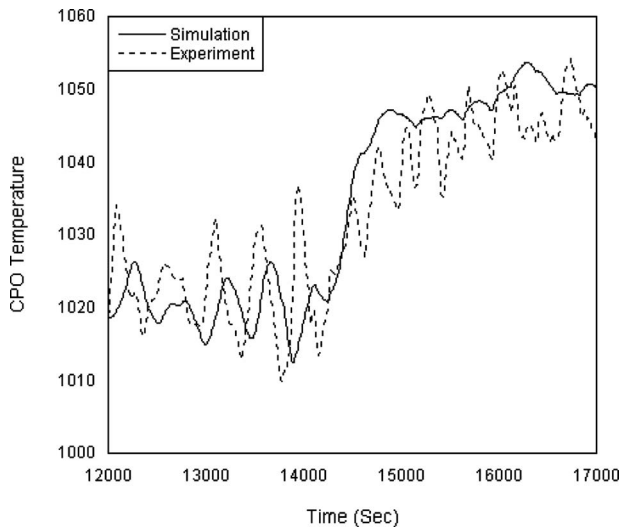
Fig. 10 Comparison of experimental and simulated transient CPO temperature response to the perturbation of Case 1
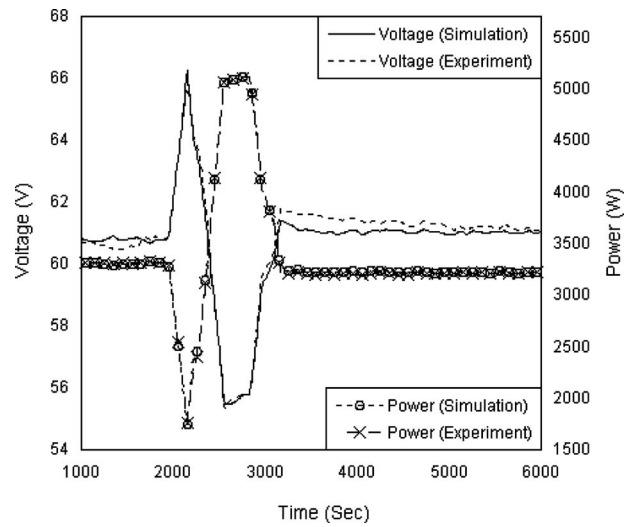
Fig. 12 Comparison of the experimental and simulated voltage and dc power response to the perturbation of Case 2

dc voltage, hydrogen utilization, and system efficiency are shown in Figs. 12 and 13, respectively. The simulation results of dynamic dc voltage and dc power are well matched with the measurement results. As the fuel flow rate during the first transient period was not decreased in proportion to the dc current, the hydrogen utilization is decreased from 0.73 to 0.42, which reduced the system efficiency to 0.21. But the fuel flow rate was well controlled during the dc current decrease from 175% to the original steady state, the system efficiency (based on stack dc current) was well maintained at a constant of 0.34.

Cases 3 and 4. During load changes, it is desirable to maintain the system efficiency. In the current case, an efficiency control strategy is developed and implemented in the stationary PEM fuel cell system model. A schematic of the proposed efficiency controller is shown in Fig. 14.

The desired fuel flow rate is determined by the controller and fuel flow efficiency and feed forward of the desired efficiency. Integral control makes it possible to track efficiency with zero steady-state error. The system efficiency is determined by dividing generated stack dc power by the energy contained in the inlet fuel,

$$e_{system} = \frac{P_{stack}}{E_{inlet}}$$

Using the current efficiency controller, the optimum fuel flow rate for maintaining a desired system efficiency can be obtained. During the transient cases 3 and 4 (corresponding to the same current perturbation as cases 1 and 2, respectively), the efficiency is maintained very closely at around 0.335, as shown in Figs. 15 and 16. During the transient default system controller, the fuel flow rate is set so that the efficiency of system varies considerably, which is shown in Figs. 17 and 18 for cases 3 and 4, respectively. Finally,
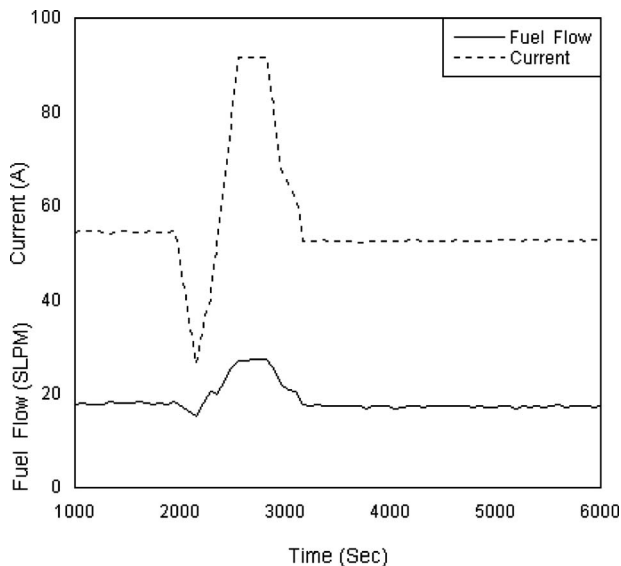
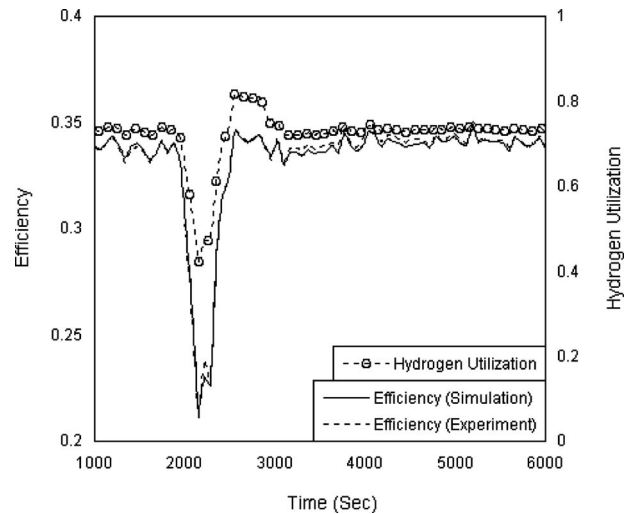**Fig. 13 Comparison of the experimental and simulated stack efficiencies and hydrogen utilization during the transient of Case 2**

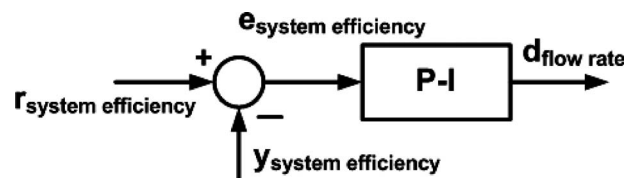**Fig. 11 dc current and fuel flow rate perturbations of Case 2**
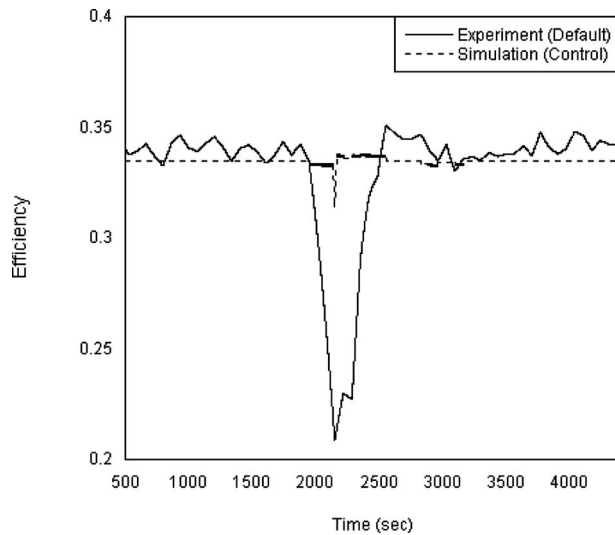
Fig. 14 Proposed system efficiency controller

Fig. 15 Comparison between the stack efficiency of the experiment (default) and simulation of the control model (control) used in Case 3

Fig. 17 Comparison of the transient experimental (default) stack efficiency and simulated (control) stack efficiency for the model of Case 4

by using this controller the accurate amount of energy is generated by optimum fuel flow rate, which prevents the system from losing the energy.

Conclusions

A dynamic model of a stationary PEM fuel cell system has been developed. The system model consists of the fuel processing system, PEM stack with coolant, humidifier with ATO, and an enthalpy wheel. For the fuel processing system, the physics and chemistry of four reactors were simulated: chemical kinetics were solved in the ATR, and the chemical equilibrium of CO with H_2O was used to solve for HTS and LTS performances. A one-dimensional dynamic PEM unit cell model was developed and used in the system model. The unit cell model contains the five control volumes of anode gas, anode GDL, electrolyte, cathode GDL, and cathode gas for solving the dynamic species and mass conservation equations. Seven 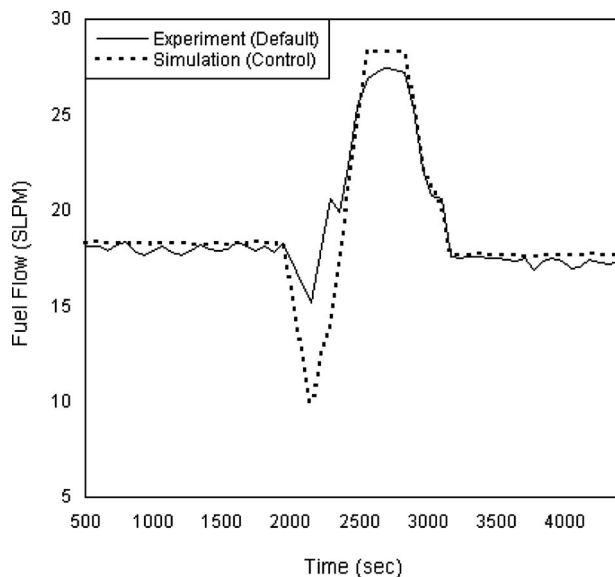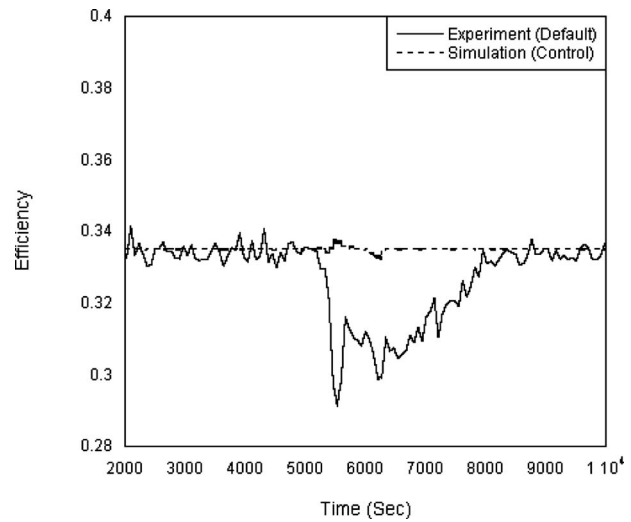control volumes of anode plate, anode, MEA, cathode, cathode plate, coolant, and end plate were used to solve the dynamic energy balance and to capture the details of MEA behavior.

A comparison of steady-state model results to experimental data shows that the system model well predicts the actual system power and CPO temperature. Transient simulation of dc power is also well matched with the experimental results to within a few percent. The model predictions well characterize the observed dynamic CPO temperature, voltage, and temperature of stack coolant outlet observations of the experiment. An efficiency controller was implemented in the model to determine and manipulate fuel flow rate to control system efficiency. The dynamic system predictions with this controller show an ability to maintain constant system efficiency during transient operation. The model is shown to be a useful tool for giving understanding regarding dynamic performance characteristics of a fuel processor and PEMFC stack and for investigating the impacts of component response characteristics on overall system dynamics. The dynamic model can also be used to develop and investigate control strategies.

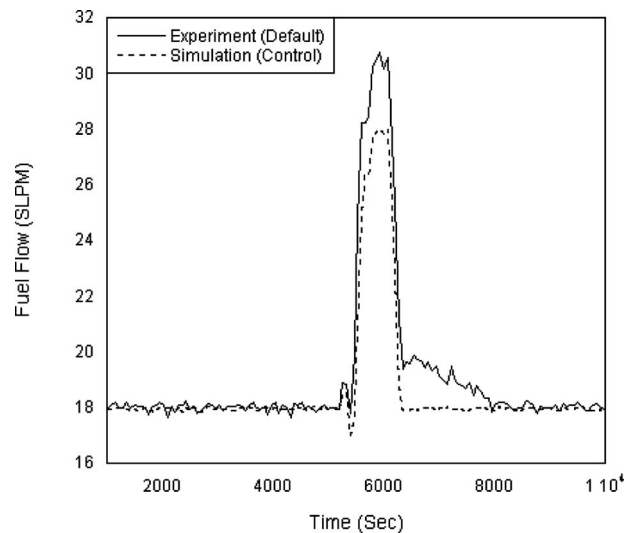**Fig. 16 Comparison between the fuel flow rate of the experiment (default) and that for simulation of control model (control) of Case 3**

Fig. 18 Comparison of the experimental (default) and simulated (control) fuel flow rate transients for Case 4

Nomenclature

A_c = convective efficient area per volume of the catalyst, 1/m

C = total molar concentration of the volume, $kmol/m^3$

C_{cata} = specific heat on a mass basis, kJ/(kg K)

$C_{v,molar}$ = specific heat at constant volume of the gas mixture on a molar basis, kJ/(kmol K)

D_m = diffusion coefficient of species m, m^2/s

F = Faraday's constant, 96,487 C/mol

g_m = mass transfer coefficient, m/s

ΔG = molar Gibbs free energy, kJ/kmol

h = enthalpy, kJ/kmol

h_c = convective coefficient between catalyst and gases.

i = local current density, A/m^2

i_o = exchange current density, A/m^2

I = current, A

$\dot{N}_{in}$ = total molar flow rate into the volume, kmol/s

L = length, m

n_d = electro-osmotic drag coefficient

$\dot{N}$ = total molar flow rate exiting the volume, kmol/s

M_{H_2O} = molecular weight of water, kg

P = pressure, kPa

P_{sat} = saturation water pressure, kPa

Q_{sg} = molar energy transfer from catalyst to gases, kw

Q_{gs} = molar energy transfer from gases to catalyst, kw

r_i = the overall reaction rate of species i

$\mathbf{R}$ = vector of individual reaction rates of the reaction

R_u = universal gas constant, 8.314 J/(mol K)

Sh = Sherwood number

t = membrane thickness, m

T_g = gas temperature, K

T_c = catalyst temperature, K

V = cell voltage, V

V_c = volume, m_3

X = direction normal to the electrolyte, m

X_{H_2O} = water mole fraction

Greek Letters

ρ = catalyst density, kg/m^3

λ = membrane water content

η_{act} = activation polarization, V

η_{Ohm} = Ohmic polarization, V

κ = proton conductivity in the membrane, S/m

ε = porosity

References

[1] Srinivasan, S., Manko, D. J., Koch, H., Enayetullah, M. A., and Appleby, J. A., 1990, "Recent Advances in Solid Polymer Electrolyte Fuel Cell Technology With Low Platinum Loading Electrodes," J. Power Sources, **29**, pp. 367–387.

[2] Ghenciu, A. F., 2002, "Review of Fuel Processing Catalysts for Hydrogen Production in PEM Fuel Cell Systems," Curr. Opin. Solid State Mater. Sci., **6**, pp. 389–399.

[3] Mehta, V., and Cooper, J. S., 2003, "Review and Analysis of PEM Fuel Cell Design and Manufacturing," J. Power Sources, **114**, pp. 32–53.

[4] Costamagna, P., and Srinivasan, S., 2001, "Quantum Jumps in the PEMFC Science and Technology From the 1960s to the Year 2000: Part II. Engineering, Technology Development and Application Aspects," J. Power Sources, **102**, pp. 242–252.

[5] Gigliucci, G., Petruzzi, L., Cerelli, E., Garzisi, A., La Mendola, A., 2004, "Demonstration of a Residential CHP System Based on PEM Fuel Cells," J. Power Sources, **131**, pp. 62–68.

[6] Boettner, D., Massie, C., and Massie, D., 2004, "Lessons Learned From Residential Experience With Proton Exchange Membrane Fuel Cell Systems for Combined Heat and Power," *Proceedings of the ASME Fuel Cell Science, Engineering, and Technology Conference*, pp. 267–272.

[7] Laosiripojana, N., Sangtongkitcharoen, W., and Assabumrungrat, S., 2006, "Catalytic Steam Reforming of Ethane and Propane Over CeO_2-Doped Ni/Al_2O_3 at SOFC Temperature: Improvement of Resistance Toward Carbon Formation by the Redox Property of Doping CeO_2," Fuel, **85**, pp. 323–332.

[8] Barrio, V. L., Schaub, G., Rohde, M., Rabe, S., Vogel, F., Cambra, J. F., Arias, P. L., and Guemez, M. B., 2007, "Reactor Modeling to Simulate Catalytic Partial Oxidation and Steam Reforming Of Methane. Comparison of Temperature Profiles and Strategies for Hot Spot Minimization," Int. J. Hydrogen Energy, **32**, pp. 1421–1428.

[9] Horng, R.-F., Chou, H.-M., Lee, C.-H., and Tsai, H.-T., 2006, "Characteristics of Hydrogen Produced by Partial Oxidation and Auto-Thermal Reforming in a Small Methanol Reformer," J. Power Sources, **161**, pp. 1225–1233.

[10] Yan, X., Wang, S., Li, X., Hou, M., Yuan, Z., Li, D., Pan, L., Zhang, C., Liu, J., Ming, P., and Yi, B., 2006, "A 75-kW Methanol Reforming Fuel Cell System," J. Power Sources, **162**, pp. 1265–1269.

[11] Zhu, J., Zhang, D., and King, K. D., 2001, "Reforming of CH_4 by Partial Oxidation: Thermodynamic and Kinetic Analyses," Fuel, **80**, pp. 899–905.

[12] Yuan, L., Brouwer, J., and Samuelsen, G. S., 2004, "Dynamic Simulation of an Autothermal Methane Reformer," Second International Conference on Fuel Cell Science, Engineering and Technology, June, ASME Paper No. FuelCell2004–2518.

[13] Leem, S., and Bae, J., 2005, "Autothermal Reforming of Natural Gas for High-Temperature Fuel Cells," Third International Conference on Fuel Cell Science, Engineering and Technology, Ypsilanti, MI.

[14] Shan, Y., and Choe, S., 2005, "Computation of Dehydration Effects of the Membrane in a PEM Fuel Cell," Third International Conference on Fuel Cell Science, Engineering and Technology, Ypsilanti, Michigan.

[15] Yuyao, S., and Choe, S.-Y., 2005, *Proceedings of the Third International Conference on Fuel Cell Science, Engineering and Technology*, Paper No. ASME FC2005–74163.

[16] Yerramalla, S., Davari, A., Feliachi, A., and Biswas, T., 2003, "Modeling and Simulation of the Dynamic Behavior of a Polymer Electrolyte Membrane Fuel Cell," J. Power Sources, **124**, pp. 104–113.

[17] Pukrushpan, T. J., Stefanopoulou, G. A., and Peng, H., 2004, *Control of Fuel Cell Power Systems Principles, Modeling, Analysis and Feedback Design*, Springer, New York.

[18] Xue, X., Tang, J., Smirnova, A., England, R., and Sammes, N., 2004, "System Level Lumped-Parameter Dynamic Modeling of PEM Fuel Cell," J. Power Sources, **133**(2), pp. 188–204.

[19] Ceraolo, M., Miulli, C., and Pozio, A., 2003, "Modelling Static and Dynamic Behaviour of Proton Exchange Membrane Fuel Cells on the Basis of Electro-Chemical Description," J. Power Sources, **113**, pp. 131–144.

[20] Wang, Y., and Wang, C., 2005, "Transient Analysis of Polymer Electrolyte Fuel Cells," Electrochim. Acta, **50**, pp. 1307–1315.

[21] Um, S., and Wang, C. Y., 2004, "Three-Dimensional Analysis of Transport and Electrochemical Reactions in Polymer Electrolyte Fuel Cells" J. Power Sources, **125**, pp. 40–50.

[22] Hu, G., Fan, J., Chen, S., Liu, Y., and Cen, K., 2004, "Three-Dimensional Numerical Analysis of Proton Exchange Membrane Fuel Cells (PEMFCs) With Conventional and Interdigitated Flow Fields," J. Power Sources, **136**, pp. 1–9.

[23] Meng, H., 2007, "A Three-Dimensional Mixed-Domain PEM Fuel Cell Model With Fully-Coupled Transport Phenomena," J. Power Sources, **164**, pp. 688–696.

[24] Maher, A. R., Sadiq, A.-B., Haroun, A. K., and Shahad, A.-J., 2007, "Parametric and Optimization Study of a PEM Fuel Cell Performance Using Three-Dimensional Computational Fluid Dynamics Model," Renewable Energy, **32**, pp. 1077–1101.

[25] Wang, Y., and Wang, C., 2006, "Dynamics of Polymer Electrolyte Fuel Cells Undergoing Load Changes," Electrochim. Acta, **51**, pp. 3924–3933.

[26] Mueller, F., Brouwer, J., Kang, S., Kim, H-S., and Min, K., 2007, "Quasi-Three Dimensional Dynamic Model of a Proton Exchange Membrane Fuel Cell for System and Controls Development," J. Power Sources, **163**, pp. 814–829.

[27] Wang, Y., and Wang, C., 2007, "Two-Phase Transients of Polymer Electrolyte Fuel Cells," J. Electrochem. Soc., **154**, pp. B636–B643.

[28] Barrio, V. L., Schaub, G., Rohde, M., Rabe, S., Vogel, F., Cambra, J. F., Arias, P. L., and Guemez, M. B., 2007, "Reactor Modeling to Simulate Catalytic Partial Oxidation and Steam Reforming of Methane. Comparison of Temperature Profiles and Strategies for Hot Spot Minimization," Int. J. Hydrogen Energy, **32**, pp. 1421–1428.

[29] Power, Plug, GenSys™ Fuel Cell System service manual, SM005.

[30] Freunberger, S. A., Santis, M., Schneider, I. A., Alexander, W., and Buchi, F. N., 2006, "In-Plane Effects in Large-Scale PEMFCs," J. Electrochem. Soc., **153**(2), pp. A396–A405.

[31] Burt, A. C., Celik, I. B., Gemmen, R. S., and Smirnov, A. V., 2004, "A Numerical Study Cell-to-Cell Variations in a SOFC Stack," J. Power Sources, **126**, pp. 76–87.

[32] Campanari, S., and Iora, P., 2004, "Definition and Sensivity of a Finite Volume SOFC Model for a Tubular Cell Geometry," J. Power Sources, **132**, pp. 113–126.

[33] Andrew, M. R., 1966, *An Introduction to Fuel Cells*, K. R. Williams, ed., Elsevier, New York.

[34] Xu, J., and Froment, G. F., 1989, "Methane Steam Reforming, Methanation and Water-Gas Shift: I. Intrinsic Kinetics," AIChE J., **35**, pp. 88–96.

[35] Jin, W., Gu, X., Li, S., Huang, P., Xu, N., and Shi, J., 2000, "Experimental and Simulation Study on a Catalyst Packed Tubular Dense Membrane Reactor for Partial Oxidation of Methane to Syngas," Chem. Eng. Sci., **55**, pp. 2617–2625.

[36] Bird, R., Stewart, W., and Lightfoot, E., 1960, *Transport Phenomena*, Wiley, New York.

[37] Springer, T., Zawodzinski, T., and Gottesfeld, S., 1991, "Polymer Electrolyte Fuel Cell Model," J. Electrochem. Soc., **136**, pp. 2334–2342.

[38] Larminie, J., and Dicks, A., 2003, *Fuel Cell Systems Explained*, 2nd ed., Wiley, New York.